# Unexpected kinetic complexity in the formation of a nonheme oxoiron(IV) complex

**Xiaopeng Shan and Lawrence Que, Jr.***

*Received (in Berkeley, CA, USA) 17th October 2007, Accepted 27th February 2008*
*First published as an Advance Article on the web 27th March 2008*
**DOI: 10.1039/b716036d**

**The stoichiometric formation of $[Fe^{IV}(O)(TPA)(NCMe)]^{2+}$ (TPA = tris(2-pyridylmethyl)amine) from the reaction of $[Fe^{II}(TPA)(NCMe)_2]^{2+}$ with 1 equiv. peracetic acid exhibits more kinetic complexity than might be expected from the simple stoichiometry. A multiple-pathway mechanism with an $Fe^{IV}$–peracetic acid species, $[(TPA)Fe^{IV}(O)((H)O_3CR)]^{2+/+}$, as the primary oxidant is proposed.**

In the last few years, nonheme oxoiron(IV) complexes have at last been synthesized and characterized.[1–3] These complexes serve as models for high-valent intermediates proposed or observed in the catalytic cycles of oxygen activating nonheme iron enzymes.[4–6] $[Fe^{IV}(O)(TPA)(NCMe)]^{2+}$, the complex supported by the tripodal TPA (tris(2-pyridylmethyl)amine) ligand represents one of the first examples of this growing family.[3] It is conveniently generated by the reaction of $[Fe^{II}(TPA)(NCMe)_2]^{2+}$ with peracid in MeCN solvent at low temperature. The observation that the addition of one equivalent of peracetic acid is sufficient to effect nearly quantitative conversion of its iron(II) precursor to the oxoiron(IV) complex would seem to suggest a straightforward mechanism depicted as pathway **A** in Scheme 1 involving O–O bond heterolysis after peracid binding to the iron(II) center. However closer examination of this reaction provides UV-Vis spectroscopic evidence strongly suggesting a more complex mechanism.

The reaction of $[Fe^{II}(TPA)(NCMe)_2]^{2+}$ (**1**) with one equivalent of peracetic acid to form $[Fe^{IV}(O)(TPA)(NCMe)]^{2+}$ (**2**) is conveniently monitored by UV-Vis-NIR spectroscopy and shown in Fig. 1. Formation of **2** is indicated by the appearance of a band near 720 nm associated with ligand field transitions of the $S = 1$ oxoiron(IV) center[7] contemporaneous with the disappearance of the 400 nm band associated with the iron(II) precursor.[3] Three isosbestic points at 445, 480, and 570 nm are observed, suggesting the straightforward conversion of **1** to **2** with no observable accumulation of an intermediate (inset of Fig. 1). At the last stage of the reaction, the formation of some fraction of the final decay product, $[Fe_2^{III}(O)(OAc)(TPA)_2]^{3+}$, which has significant absorption in the range of 425–550 nm, results in the spectrum represented by the black line in Fig. 1.

Fig. 2A shows changes in the absorbances at 435, 480 and 720 nm as a function of time. These wavelengths were chosen to monitor, respectively the disappearance of **1**, an isosbestic point in the conversion of **1** to **2**, and the formation of **2**. The plot reveals the decrease of the 435 nm absorbance concurrent with the increase of the 720 nm absorbance. Interestingly, both absorbance traces at 435 and 720 nm show an elongated induction phase at the initial stage, then a sharp acceleration to a plateau at the final stage, while the absorbance at 480 nm stays constant during the formation of **2**. This behavior can be rationalized by an autocatalytic mechanism in which the product catalyzes its own formation.

To gain further insight into the complexity of this reaction, two experiments were conducted and monitored at the same three wavelengths. In the first experiment, **1** was reacted with 0.5 equiv. peracetic acid. After 300 s, the stoichiometric formation of 0.5 equiv. **2** was observed; then another 0.5 equiv. peracetic acid was introduced into the reaction mixture. Fig. 2B shows that the induction phase found in the formation of **2** after the addition of the first aliquot of peracetic acid was not observed upon addition of the second aliquot. In a second experiment, addition of a large excess of peracetic acid ($\sim$10 equiv.) into a solution of **1** resulted in the stoichiometric formation of **2** within 50 s (Fig. 2C). The absorbance at 720 nm then decreased in intensity by a few percent and returned to its maximum value over a period of 100 s. Concomitantly, the absorbances at 435 and 480 nm increased after the initial 50 s time period and declined to their values at 50 s; the observed absorbance changes at 435 and 480 nm differ significantly from those observed with stoichiometric peracid in Fig. 2A and B. This behavior suggests the formation

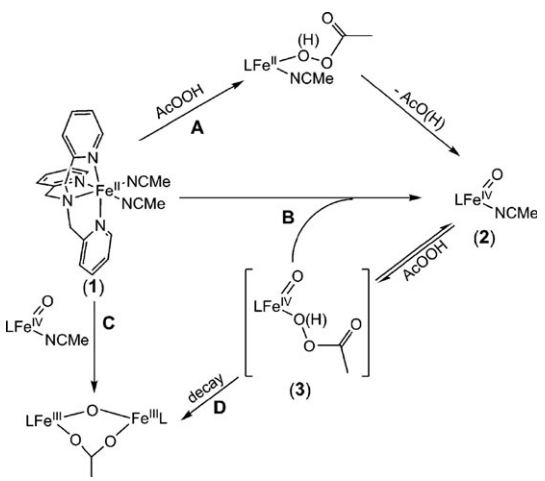


**Scheme 1** Proposed mechanism of formation of $[Fe^{IV}(O)(TPA)(NCMe)]^{2+}$ (**2**).

*Department of Chemistry and Center for Metals in Biocatalysis, University of Minnesota, Minneapolis, Minnesota 55455, USA. E-mail: larryque@umn.edu; Fax: +1 612 624 7029; Tel: +1 612 625 0389*

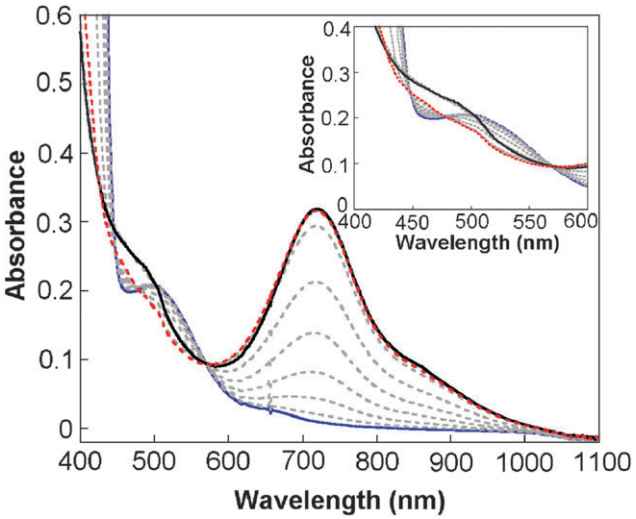


**Fig. 1** Formation of $[Fe^{IV}(O)(TPA)(NCMe)]^{2+}$ (**2**) (red) from the reaction of 1 mM $[Fe^{II}(TPA)(NCMe)_2]^{2+}$ (**1**) (blue) with one equivalent of peracetic acid in MeCN at −40 °C. Inset: Magnified view of 400–600 nm range.

of a subsequent species (designated as **3**) with an absorbance feature near 450 nm that is in equilibrium with **2**, consumes the remaining free peracetic acid, and reverts to **2** upon depletion of the excess peracid.

A mechanistic scheme can be proposed on the basis of the evidence described above (Scheme 1). Four pathways are involved in this reaction. Pathway **A** is the straightforward pathway, which is responsible for the slow initial generation of **2** *via* O–O bond heterolysis. Pathway **B** is the major pathway for the formation of **2**, in which peracetic acid binds to the initially formed **2** to form an adduct, **3**, that rapidly reacts with residual **1** to yield two molecules of **2**. Pathway **D** is the termination step of the catalytic cycle, giving rise to the final UV-Vis increase around 500 nm in Fig. 1 associated with the formation of the (μ-oxo)diiron(III) byproduct. Another possible side reaction is the reaction of **2** with **1** to form a (μ-oxo)diiron(III) product (pathway **C**). This reaction was investigated separately by reacting 1 mM **2** with a 10-fold excess of **1**. Given that this reaction took 100 s to achieve completion, it is not likely that pathway **C** plays any role in the reaction of **2** with stoichiometric peracid, owing to the low concentrations of **1** and **2** present.

To test the proposed mechanism in Scheme 1, a kinetic simulation was carried out with KINSIM software (http://www.biochem.wustl.edu/cflab/message.html). By using parameters listed in the caption of Fig. 3, concentration change curves comparable to those found in our experiment were achieved within the experimental time scale. The use of these parameters simulates three features observed in Fig. 2A: the initial extended lag phase, the subsequent linear phase, and the final sharp transition to a plateau, demonstrating that Scheme 1 is not an unreasonable model for our observations. To achieve the desired simulation required a slight excess of peracid. Experimentally, this slight excess may be provided by the residual $H_2O_2$ present in commercially available 32% peracetic acid solutions in acetic acid. Unfortunately, there are

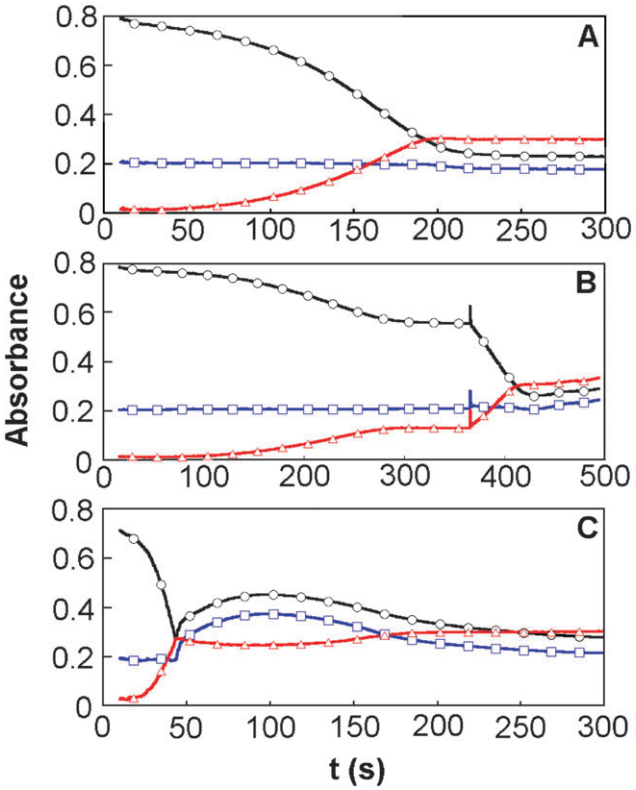


**Fig. 2** Plots of absorbance changes at 435 (black circles), 480 (blue squares), and 720 (red triangles) nm for the reaction of 1 mM $[Fe^{II}(TPA)(NCMe)_2]^{2+}$ (**1**) with different amounts of peracetic acid in MeCN at −40 °C: (A) one equivalent added all at once; (B) stepwise addition of two half-equivalents; and (C) ten equivalents added all at once.

too few observables in the current data set to allow us to pin down the rate constants more precisely.

Based on Scheme 1, we propose that the primary oxidant in this system is an adduct of $[(TPA)Fe^{IV}(O)(solv)]^{2+}$ and $HO_3CR$, formulated as $[(TPA)Fe^{IV}(O)((H)O_3CR)]^{2+/+}$ (**3**), with a structure related to a well-characterized $Fe^{IV}$-peroxo

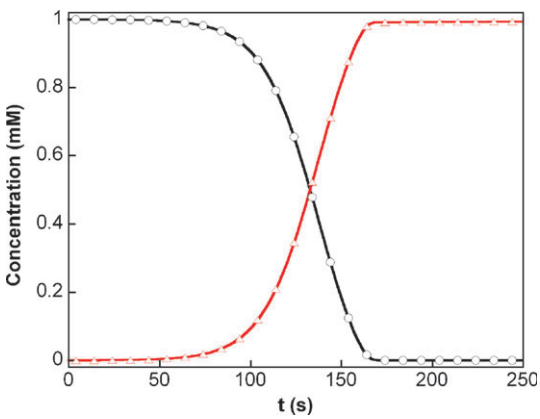


**Fig. 3** Plots of concentration changes of **1** (black circles) and **2** (red triangles) for the reaction of **1** with peracetic acid simulated by using KINSIM software with the following parameters: [**1**] = 1.0 mM, [peracetic acid] = 1.2 mM, $k$(pathway **A**) = $1 \times 10^{-3}$ $M^{-1}$ $s^{-1}$, $k$(**2** → **3**) = 50 $M^{-1}$ $s^{-1}$, $k$(**3** → **2**) = 1 $s^{-1}$, $k$(pathway **B**) = $1 \times 10^{6}$ $M^{-1}$ $s^{-1}$.

species, $[(BPMCN)Fe^{IV}(OH)(OO^tBu)]^{2+}$ (BPMCN = *N*,*N*′-bis(2-pyridylmethyl)-*trans*-1,2-diaminocyclohexane).[8] The addition of $HO_3CR$ enhances the oxidation power of **2** by two oxidizing equivalents, so it is reasonable to propose that **3** is a more powerful oxidant and a better oxygen atom transfer reagent than **2**. Moreover, since the $Fe^{IV}$ ion in **2** may be expected to be a much stronger Lewis acid than the corresponding $Fe^{II}$ center in **1**, it should be more effective in promoting O–O bond cleavage, just like $V^V$ and $Mn^{IV}$ centers that activate $^t$BuOOH for olefin epoxidation.[9,10] Indeed, some oxoiron(IV) and oxomanganese(V) complexes have been reported to activate PhIO for oxygen atom transfer to organic substrates.[11,12] Furthermore, examples of oxoiron(V), nitridoiron(V) and nitridoiron(VI) complexes have been characterized for nonheme macrocyclic ligands.[13–15] For tripodal TPA, it has been proposed that $Fe^V{=}O$ species act as the oxidants in the hydroxylation of alkanes and the epoxidation and *cis*-dihydroxylation of olefins by Fe(TPA) catalysts.[16–18] Our results thus open the door to the possibility that even higher valent Fe(TPA) complexes may be accessed or trapped.

This work was supported by National Institutes of Health Grant GM-33162.

## Notes and references

1 X. Shan and L. Que, Jr., *J. Inorg. Biochem.*, 2006, **100**, 421–433.
2 J.-U. Rohde, J.-H. In, M. H. Lim, W. W. Brennessel, M. R. Bukowski, A. Stubna, E. Münck, W. Nam and L. Que, Jr., *Science*, 2003, **299**, 1037–1039.
3 M. H. Lim, J.-U. Rohde, A. Stubna, M. R. Bukowski, M. Costas, R. Y. N. Ho, E. Munck, W. Nam and L. Que, Jr., *Proc. Natl. Acad. Sci. U. S. A.*, 2003, **100**, 3665–3670.
4 J. M. Bollinger, Jr. and C. Krebs, *J. Inorg. Biochem.*, 2006, **100**, 586–605.
5 M. Costas, M. P. Mehn, M. P. Jensen and L. Que, Jr., *Chem. Rev.*, 2004, **104**, 939–986.
6 M. M. Abu-Omar, A. Loaiza and N. Hontzeas, *Chem. Rev.*, 2005, **105**, 2227–2252.
7 A. Decker, J.-U. Rohde, L. Que, Jr. and E. I. Solomon, *J. Am. Chem. Soc.*, 2004, **126**, 5378–5379.
8 M. P. Jensen, M. Costas, R. Y. N. Ho, J. Kaizer, A. M. Payeras, E. Münck, L. Que, Jr., J.-U. Rohde and A. Stubna, *J. Am. Chem. Soc.*, 2005, **127**, 10512–10525.
9 M. Greb, J. Hartung, F. Koehler, K. Spehar, R. Kluge and R. Csuk, *Eur. J. Org. Chem.*, 2004, 3799–3812.
10 G. Yin, A. M. Danby, E. Kitko, J. D. Carter, W. M. Scheper and D. H. Busch, *Inorg. Chem.*, 2007, **46**, 2173–2180.
11 Y. Suh, M. S. Seo, K. M. Kim, Y. S. Kim, H. G. Jang, T. Tosha, T. Kitagawa, J. Kim and W. Nam, *J. Inorg. Biochem.*, 2006, **100**, 627–633.
12 S. H. Wang, B. S. Mandimutsira, R. Todd, B. Ramdhanie, J. P. Fox and D. P. Goldberg, *J. Am. Chem. Soc.*, 2004, **126**, 18–19.
13 F. Tiago de Oliveira, A. Chanda, D. Banerjee, X. Shan, S. Mondal, L. Que, Jr., E. L. Bominaar, E. Münck and T. J. Collins, *Science*, 2007, **315**, 835–838.
14 K. Meyer, E. Bill, B. Mienert, T. Weyhermüller and K. Wieghardt, *J. Am. Chem. Soc.*, 1999, **121**, 4859–4876.
15 J. F. Berry, E. Bill, E. Bothe, S. D. George, B. Mienert, F. Neese and K. Wieghardt, *Science*, 2006, **312**, 1937–1941.
16 K. Chen and L. Que, Jr., *J. Am. Chem. Soc.*, 2001, **123**, 6327–6337.
17 K. Chen, M. Costas, J. Kim, A. K. Tipton and L. Que, Jr., *J. Am. Chem. Soc.*, 2002, **124**, 3026–3035.
18 R. Mas-Ballesté and L. Que, Jr., *J. Am. Chem. Soc.*, 2007, **129**, 15964–15972.